ISSN 1068-3755, Surface Engineering and Applied Electrochemistry, 2015, Vol. 51, No. 4, pp. 367–373. © Allerton Press, Inc., 2015.

Study of Hot Corrosion Resistance of Electroless Nickel Coating with Different Content of Phosphorous in Molten Salt Deposit Na_2SO_4–NaCl at 650°C[1]

M. Ghaderi[a, *], M. Rezagholizadeh[a], H. Nasiri-Vatan[b], and R. Ebrahimi-Kahrizsangi[b]

[a] *Young Researchers and Elite Club, Najafabad Branch, Islamic Azad University, Najafabad, Iran*

[b] *Materials Engineering Department, Najafabad Branch, Islamic Azad University, Najafabad, Isfahan, Iran*

e-mail: mo.ghaderi@yahoo.com

Received June 10, 2014; in final form, July 28, 2014

Abstract—In this research, the hot corrosion behavior of electroless nickel-(4, 7, 9, and 12 wt % P) was studied in 70 wt % Na_2SO_4–30 wt % NaCl (3 and 6 mg/cm^2) molten salt on a copper substrate. After being plated with a thickness of 25 ± 3 μm, the specimens were annealed at 400°C for 1 hour, and then the hardness of each was measured by the Vickers hardness test method. The hot corrosion test was performed at 650°C for 20 hours inside the furnace at a rate of 4°C/min under atmospheric conditions. The results showed that Ni–7 wt % P and Ni–12 wt % P electroless coatings included the highest and the lowest hot corrosion resistance, respectively. The difference in the weight increase of the hot corrosion of Ni–12 wt % P coating was about 8 times as much as that of Ni–7 wt % P, and the difference in thermal expansion between the substrate and the coating was responsible for the cracks in the coating. Diffusion of the molten salt through these cracks expanded and reached the intersection of the coating and the substrate. The results of the XRD showed the formation of $NiSO_4$, NiO, and Cu on the coating surface after the hot corrosion test.

Keywords: electroless, Ni–P, molten salt, hot corrosion, hot mount

DOI: 10.3103/S1068375515040055

1. INTRODUCTION

Electroless Ni–P alloy coatings have found extensive industrial applications due to their unique properties such as corrosion [1] and wear resistance [2], high hardness [3] and uniformity of the coating thickness [4]. Corrosion properties of electroless Ni–P coatings depend on the phosphorous content and the consequent structural and mechanical state. The electroless Ni–P alloy plating with 5–10 wt % of the P content exhibits a microcrystalline, partly amorphous, structure [5] or, depending on the composition and operating conditions of the deposition bath and the P content above 8 wt %, the coatings have no crystalline structure.

Modern blast furnaces may have up to 42 tuyeres [6] for the injection of the hot blast into the furnace Corrosion caused by the salt molten deposition is the most significant drawback of these tuyeres that are usually made from copper. The reaction between sodium chloride and metals with oxygen causes the formation of volatile metal chlorides, which results in a severe high-temperature corrosion [7]. Therefore, developing coatings that could hinder NaCl or chlorine attack is a serious and challenging requirement. Studies on hot corrosion induced by NaCl/Na_2SO_4 mixtures have commonly focused on Ni–Cr and other super alloys used in tuyeres [8]. The nickel-based alloys are capable of withstanding chloride attack and exhibit a superior corrosion resistance compared to that of other metals [9]. Also, an electroless nickel plating has been used as a functional coating due to its advantages such as corrosion and wear resistance. Hence, a possibility of using the electroless nickel coating in a NaCl-containing environment is an intriguing issue [10, 11].

In this study, the hot corrosion behavior of the electroless nickel coatings with different phosphorous content is studied. Hot corrosion occurs as a result of using low quality fuels that contain impurities such as Na, S, and Cl that form Na_2SO_4 and NaCl salts on the surface of tuyeres and cause a corrosive attack.

2. EXPERIMENTS

Four specimens with dimensions of 1 × 1 × 0.2 cm of Cu-DHP (Deoxidation High Phosphorous) and wt % P = 0.015 and wt % Cu = 99.9 were cut. The specimens were grit blasted up to 600 degrees; and in order to have more roughness, they were sandblasted. To prevent the reaction of other parts of the specimens and errors in the weight measurement, the specimens

[1] The article is published in the original.

Elearnica Downloaded from http://www.elearnica.ir

Table 1. Bath composition and electroless plating parameters

Composition	Quantity, g L^{-1}
Nickel sulfate ($NiSO_4 \cdot 6H_2O$)	25
Sodium hypophosphite ($Na_2H_2PO_2 \cdot H_2O$)	25
Sodium citrate ($Na_3C_6H_5O_7 \cdot 2H_2O$)	50
Ammonium sulfate ($(NH_4)_2SO_4$)	28
Lactic acid ($C_3H_6O_3$)	5
Lead acetate ($Pb(C_2H_3O_2)_2$)	2
Temperature	85 ± 2°C
Time	1.5 to 4.5 h

Table 2. Influence of pH value bath on the microhardness of coatings

pH bath	Time of plating (h)	wt % P	wt % Ni	Hardness (HV_{100}) ± 5
4	4.5	12	88	740
4.5	3	9	91	850
5.5	2	7	93	930
6	1.5	4	96	1050

were separately molded in epoxy and were ready for plating in an electroless bath. Table 1 shows the chemical composition of the coating bath. The temperature of the bath was 82°C. The specimens were annealed at °C for one hour before hot corrosion testing. Table 2 shows the details of the hardness of the electroless coatings.

The hot corrosion resistance test was carried out at 650°C for 20 hours in a supersaturated solution of 70 wt % Na_2SO_4 and 30 wt % NaCl in water by the dipping method. The amount of the salt deposited on the surface of the specimens was examined at two groups. The first and the second group each contained 3 and 6 mg/cm^2 of the above salt solution on the surface of the coating, respectively. The surfaces of the plated specimens were placed in contact with the salt solution and were then heated in an oven at 120°C for 1 hour. After removing the water and the slat cover deposit from the surface of the coating, the specimens were weighed. The amount of the deposited salt for each specimen was 3 ± 0.2 mg/cm^2. For the second group, four other specimens similar to those of the first group were placed beside the supersaturated salt solution composition again after drying. The salt deposit in these specimens was 6 ± 0.2 mg/cm^2. The samples weight change during hot corrosion was calculated within the time intervals of 1, 2, 4, 10, 15, and 20 hours. They were measured three times and their average weight was reported. The heating rate was selected to be 4°C/min for the corrosion test. This temperature was selected because of the salt solution is liquid on the surface of the coating. The eutectic temperature for the fusion of the salt composition under testing was 629°C [12].

A scanning electron microscope (SEM) was used to study the cross-section morphologies of the coatings after hot corrosion testing. The chemical composition was analyzed through energy dispersive X-ray spectroscope attached to the SEM. The X-ray diffraction (XRD) analysis was performed the after hot corrosion testing.

3. RESULTS AND DISCUSSION

The thickness of the coatings was about 25 ± 3 μm. The specimens were coated with different pH values in the Ni electroless bath. The energy-dispersive X-ray spectroscopic (EDS) analysis showed the quantity of phosphorous along with the pH change for each specimen as given in Table 2. With an increase in the amount of phosphorous after annealing at 400°C, the coating hardness gradually decreased. The images of the cross sections of the specimens after the hot corrosion test for both the first and the second group of nickel electro-less coatings with 4, 7, 9 and 12 wt % phosphorous are shown in Figs. 1 and 2, respectively. As is observed, the mixture of the molten salt on the surface makes cracks and destruct the coating under the effect of temperature after 20 hours. The rate of the destruction of the coating is accompanied with changes in the content of phosphorous. The molten salt on the coating surface penetrates into the coating and makes cracks in it. The intensity of destruction has been instrumental in the separation of the coating from the substrate in some of the specimens. Elemental distribution after hot corrosion studies for electroless coatings in first group are illustrated in Fig. 6. These images show that the penetration of oxygen into the coating is changed with changes in the coating alloy. Copper has also penetrated into the coating from the substrate. Figure 4 shows the diagram for the results of changes in the coating weight over specific time intervals. The results of an increase in the weight of 4 to 12 wt % phosphorous nickel electroless coatings for both groups showed that the Ni–7wt%P electroless specimens had the least weight increase, while specimens 4 and 12 showed the highest weight increase. Figure 5 shows the XRD results of the Ni–P electroless coating surface after the hot corrosion test where the $NiSO_4$ and NiO phases are formed on the surface of the coating. Also, by following the path of the copper inside the coating (Fig. 3) and with the formation of CuO phase on the coating surface (Fig. 5), it is possible to distinguish the penetration of copper onto the surface of the coating through the coating cracks.

The cracks produced on the specimens of the first group during the corrosion test are the ways of the penetration of copper into the cracks of the coating, thus producing some cavities in certain sections of the substrate. The movements of copper towards the coating

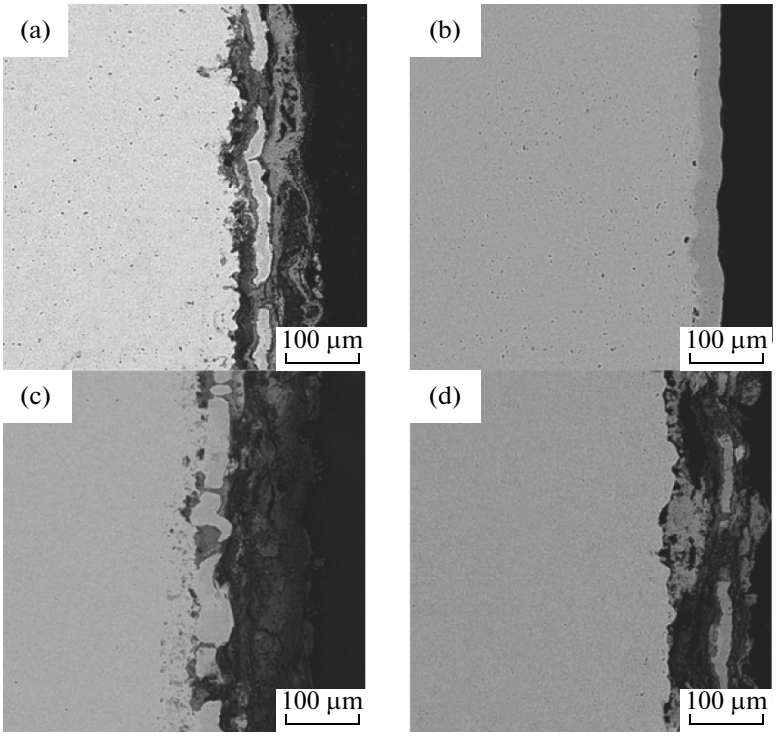

Fig. 1. Cross-sectional back scattered images of (a) Ni–4 wt % P; (b) Ni–7 wt % P; (c) Ni–9 wt % P; (d) Ni–12 wt % P subjected to 3 mg/cm^2 70 wt % Na_2SO_4 + 30 wt % NaCl at 650°C for 20 h (first group).

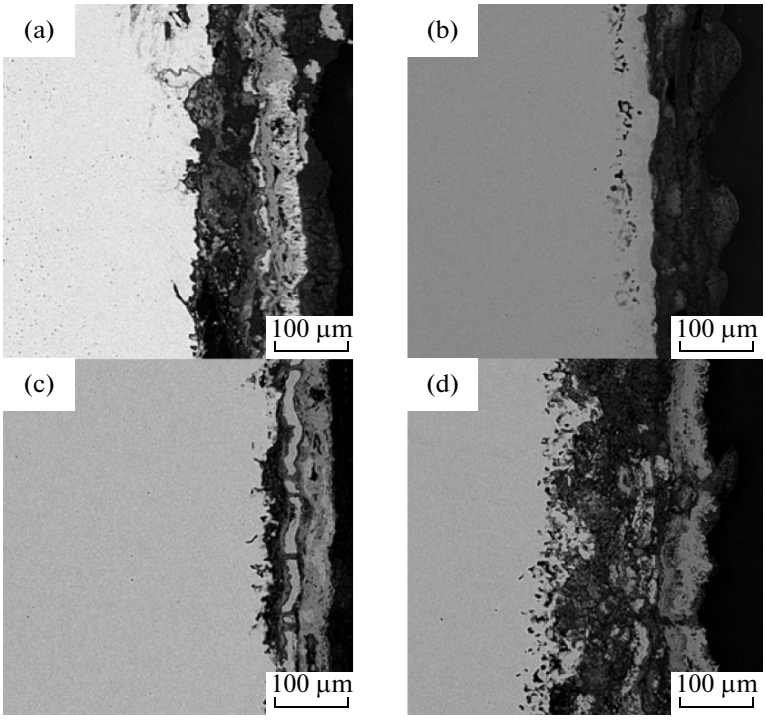

Fig. 2. Cross-sectional back scattered images of (a) Ni–4 wt % P; (b) Ni–7 wt % P; (c) Ni–9 wt % P; (d) Ni–12 wt % P subjected to 6 mg/cm^2 70 wt % Na_2SO_4 + 30 wt % NaCl at 650°C for 20 h (second group).

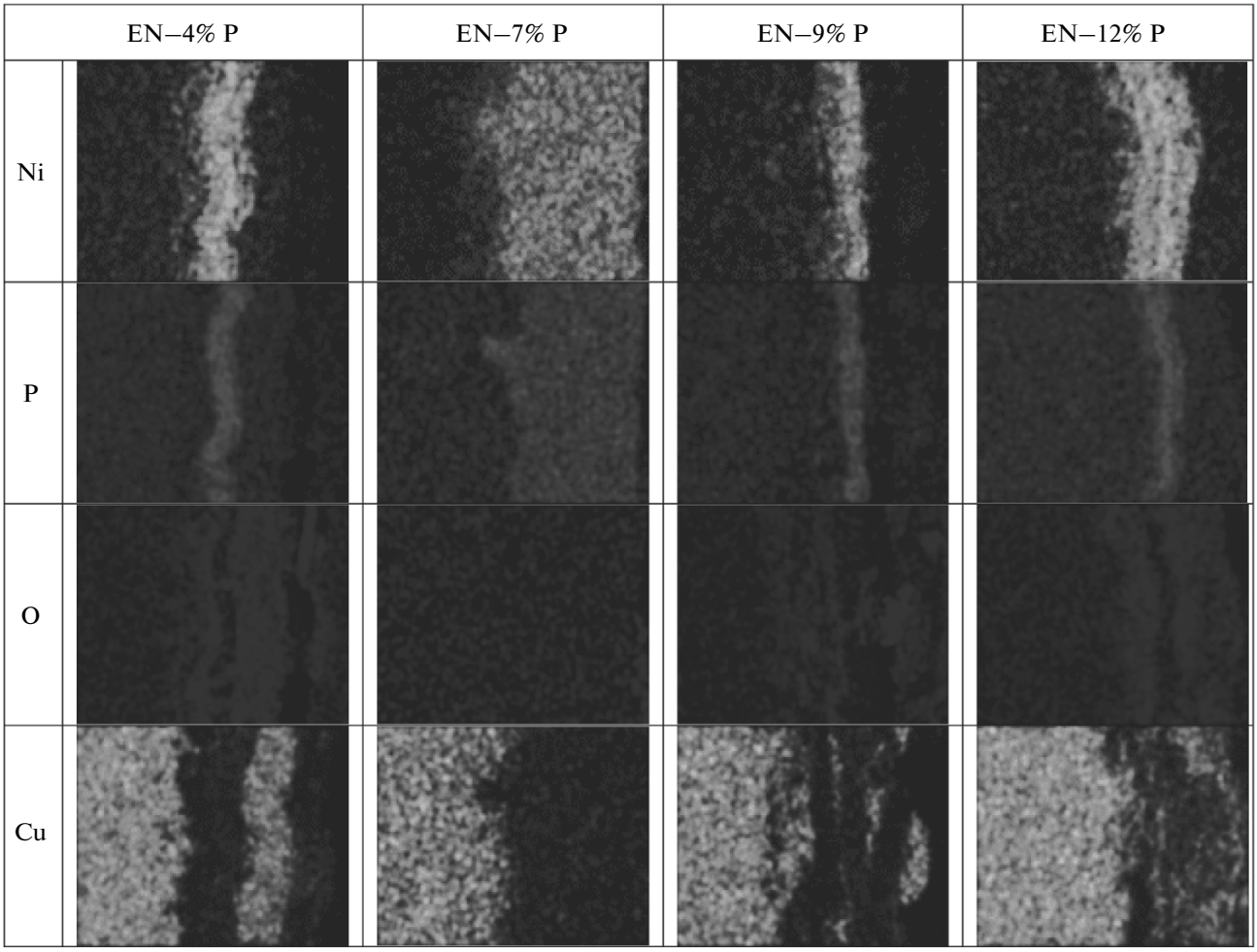

Fig. 3. X-ray mappings of electroless coating after exposure of 20 h in 70 wt % Na_2SO_4 + 30 wt % NaCl (first group).

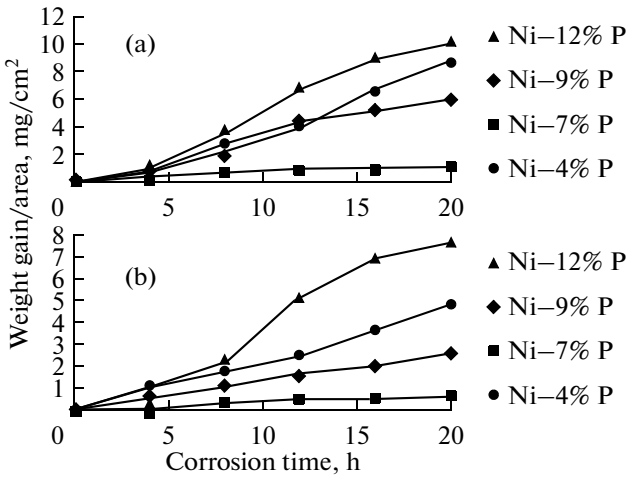

Fig. 4. Weight gain for electroless coatings Ni–4,7,9 and 12 wt % P; (a) 3 mg/cm^2 70 wt % Na_2SO_4 + 30 wt % NaCl; (b) 6 mg/cm^2 70 wt % Na_2SO_4 + 30 wt % NaCl at 650°C for 20 h (first group).

cracks and also the diffusion of nickel present inside the coating towards the substrate are observable in the X-ray mapping figures. It seems that copper penetrates mostly through the cracks in the mold coating, so that no mount is observed inside the coating of the concentration gradient of copper of the substrate interface (substrate-coating to coating-mount); while the coating surface contains a considerable amount of copper. It is observed in the corrosion testing of the second group that the coating is heavily under the effect of corrosive materials and becomes brittle. A great number of the porosities existing in the coating shows that the resistance to hot corrosion in Ni–4 wt % P electroless coating is reduced from 3 to 6 mg/cm^2 with an increase in corrosive materials. According to Table 2, the Ni–4 wt % P electroless coating is the hardest coating among other investigated coatings. The number of intermetallic phases of nickel phosphide is less than that of other specimens with a higher content of phosphorous [13–15]. Also, with an increase in the content of phosphorous, the linear expansion coefficient is reduced. The linear expansion coefficient of

Ni–4 wt % P electroless coating contains 24 m/m°C and the substrate has 16.5 m/m°C [16]. Therefore, the stress resulting from the thermal expansion of the coating and the substrate results in the production of stress and ultimately cracks in the coating. In electroless Ni–7 wt % P specimens it is evident that the resistance of this coating against hot corrosion is higher than that of other specimens. Figure 3 shows that nickel and copper have penetrated into the substrate and coating up to a small depth, respectively. Since the melting point of copper (1084°C) is lower than that of nickel (1455°C), the penetration activity of copper into nickel is more active than that of nickel into copper as specified in X-ray mapping (Fig. 3); since there are no cracks in the coating, the penetration of oxygen into it has been very little. The change in the weight of the Ni–7 wt % P specimen for both groups was approximately constant. Therefore, the Ni–7 wt % P electroless specimens show a higher resistance against hot corrosion in the molten salt. The linear expansion coefficient for the Ni–7 wt % P alloy is about 17 m/m°C which has a close conformity with the substrate of the coating [17, 18]. Therefore, no breakage resulting from the thermal expansion difference has taken place and the corrosive materials have not penetrated into the interface of the coating and the substrate. By comparing X-ray mapping images of nickel and copper, it is possible to observe that both the depth of the copper penetration into the coating and the depth of nickel penetration into the substrate have increased with an increase in the quantity of the coating phosphorous.

At hot corrosion, the Ni–9 wt % P coating in the first group is cracked, and some micro-cavities are produced in the substrate. The presence of micro-cavities in the substrate brings about more active penetration of copper into the coating, but the coating still preserves its cohesion with the substrate. The X-ray mapping (Fig. 3) show that copper that penetrated from the substrate into the coating has produced a cavity in the substrate. On the other hand, many cracks have been produced in the coating of the second-group at hot corrosion, and the coating has been separated from the substrate. Figure 4 shows the diagram of the weight change with a small increase in the gradient where the hot corrosion of the first and the second groups shows a weight increase of 2.5 and 5.9 mg, respectively. The linear expansion coefficient of this coating is about 15 m/m°C [16], so the linear expansion coefficient difference between the coating and the substrate results in the coating cracks.

Now compare the images of Ni–12 wt % P electroless specimens with those of other specimens taken by the X-ray mapping and SEM (Figs. 1–3). It seems that the coating is more porous and shows lower corrosion resistance than that Ni–9 wt % P. In Ni–12 wt % P electroless specimens, coating is separated from substrate and the amount of oxygen has increased between these two layers forming an oxide. Destruction of the first group specimen has brought about deep cracks in the coating where corrosion products are collected both in the interface of the coating and the substrate. The diagram in Fig. 4 shows where the highest weight belongs to Ni–12 wt % P. The linear expansion coefficient of Ni–12 wt % P is about 10 m/m°C. The difference between the expansion coefficient of the coating and the substrate is about 6.5 m/m°C bringing about a great deal of stress in the interface. The reason for a higher corrosion resistance, in fact, lies in close values of the thermal expansion coefficients of the coating and the substrate, which prevents cracking of coating during the hot corrosion test. In addition, the structure of the high-phosphorous coating includes most phases of nickel phosphide [19]; and according to the X-ray mapping images, the element of copper inside the coating has penetrated deeper.

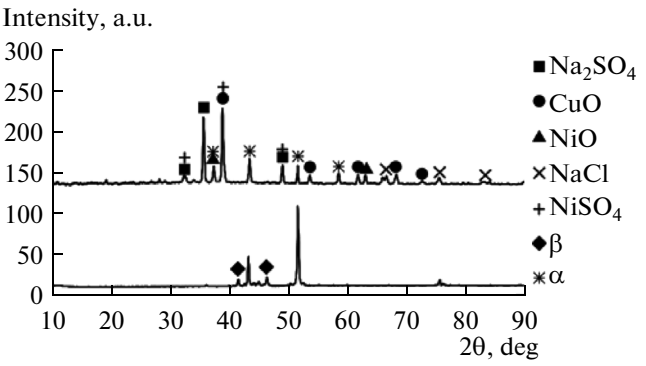

Fig. 5. X-ray diffraction patterns of electroless coating after hot corrosion testing at 650°C for 20 h.

With an increase in the quantity of phosphorous, many intermetallic phases are formed [20–22]. Research shows that when applying heat treatment at 400°C for one hour on the low-phosphorous nickel electroless coating and on high-phosphorous nickel electroless coating, 23 and 44 intermetallic phases are observed, respectively [23]. Formation of multiple phases brings about changes in the mechanical and physical properties of the coating. As it evident in Table 2, the hardness of Ni–(4, 7, 9, and 12 wt % P) electroless coating after heat treatment is 740, 850, 930, and 1050 HV, respectively. With an increase in the content of phosphorous in the coating, its hardness decreases gradually, because the nickel phosphide phases (β) have lower hardness relative to that of the crystalline nickel (α) [23]. On the other hand, with an increase in the amount of phosphorous, the temperature of the Ni–P electroless coating annealing is reduced [24]. Since the coatings have been under the temperature of 650°C for 20 hours, the unstable phases of nickel phosphide such as Ni_7P_3 and $Ni_{12}P_5$ are changed into Ni_3P stable phases, and a long period of testing has brought about coarsening of the grains [23]. Figure 6 shows the SEM image of the cross sec-

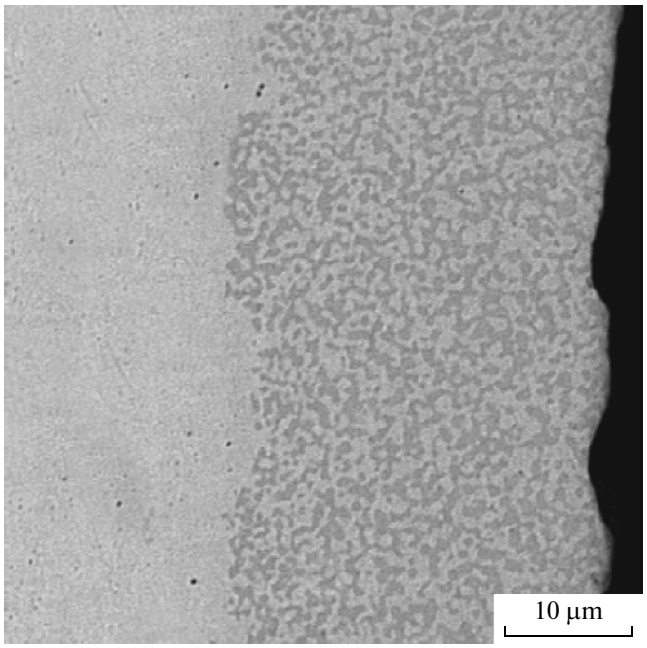

Fig. 6. SEM image of cross-section of Ni–7 wt % P coating after hot corrosion testing.

tion of the etched Ni–7 wt % P electroless coating without the addition of salt in hot corrosion testing. As is obvious, the coating grains have grown after 20 hours at 650°C. Therefore, with an increase in the content of the coating phosphorous, the amount of the secondary phase (β) and the penetration of the aggressive ions increase in the coating. Also, the linear expansion coefficient is one of the variable parameters in the nickel electroless coating with a different content of phosphorous. With an increase in the content of phosphorous, the linear expansion coefficient of the coating gradually increases. The thermal expansion coefficients of copper and nickel electroless coatings with about 7 wt % of phosphorous expand at the same pace, preventing the cracking of the coating. Likewise, the high-phosphorous electroless coating will be under tensile stress conditions with less thermal expansion than that of the substrate leading to cracking and separation of the interface of the coating and substrate. A higher thermal expansion of the low-phosphorous electroless coating relative to that of the substrate results in the shear stress at the interface leading to its separation. With the production of mechanical cracks in the coating, the path for the aggressive penetration of ions into the interface is facilitated more. The results of the XRD of the surface of coatings shows that nickel (α) has changed into NiO. Also, according to Eqs. (2) and (3), $NaSO_4$ has decomposed into sulfate and sul-fite sequentially and ultimately it forms the $NiSO_4$ phase (Eq. (4)) with nickel oxide. Also, the XRD image shows the curve of the CuO phase at the coating surface (Fig. 5). The XRD pattern in the as-plating condition is amorphous. As can be seen in Fig. 5, after annealing only the peaks reflecting α and β phases have appeared. The intermetallic compound of Ni_3P (β) is created due to heat treatment of the coating [23]. According to X-ray mapping images, the intensity of the penetration of copper into the coating surface increases with an increase in the content of the coating phosphorous, thus resulting in an increase in the weight of the high-phosphorous specimens. The NaCl and Na_2SO_4 phases remaining on the coating surface are distinguishable in the XRD results.

$$Na_2SO_4^{(s)} \rightarrow 2Na + SO_3^{(g)} + 1/2O_2, \quad (1)$$

$$Ni^{(s)} + 1/2O_2 \rightarrow NiO^{(s)}, \quad (2)$$

$$SO_3^{(g)} + H_2O^{(g)} \rightarrow H_2SO_4^{(g)}, \quad (3)$$

$$H_2SO_4 + NiO \rightarrow NiSO_4^{(s)} + H_2O. \quad (4)$$

4. CONCLUSIONS

In principle, the thermal expansion coefficient of an electroless Ni–P coating is decreasing with an increase of the phosphorous content, becoming close to that of the substrate when the concentration of phosphorous reaches 7 wt % providing the best corrosion protection due lowest stresses followed by lowest cracking under high temperatures.

The amplitude of the thermal expansion coefficient of the Ni–P electroless coating is extensive, so we can specify the alloy composition of the electro-less coating according to the thermal expansion coefficient of the substrate and use it in pieces exposed to hot corrosion in industry. An increase in the difference between the thermal expansion of the coating and the substrate results in the breakage of the coating and separation of the interface of the coating-substrate. The presence of oxygen and sulfur compounds like Na_2SO_4 leads to the formation of NiO and Ni_2SO_4 phases in the cracks and the interface of coating-substrate so that the coating loses it efficiency.

The change in the content of phosphorous also has a great effect on the structure and the amount of the secondary phase. An increase in phosphorous lessens the coating purity and reduces its resistance to hot corrosion. The depth of copper penetration into the coating increases with an increase in the content of the coating phosphorous, and the CuO phase also increases. The highest weight increase is in Ni–12 wt % P, while the lowest is in the Ni–7 wt % P electroless specimen. The factor of the weight increase of the coatings is the formation of NiO, CuO, and $NiSO_4$ phases.

REFERENCES

1. Hiratsuka, K., Abe, Y., and Kawashima, S., Effect of in-situ electroless plating on friction and wear of metals, *Wear*, 2003, vol. 255, nos. 7–12, pp. 910–916.
2. Li, Z.-H., Chen Zhi-yong, Liu Sha-sha, Zheng Feng, and Dai A-gan, Corrosion and wear properties of electroless Ni–P plating layer on AZ91D magnesium alloy, *T. Nonferr. Metal. Soc.,* 2008, vol. 18, no. 4, pp. 819–824.
3. Subramanian, C., Cavallaro, G., and Winkelman, G., Wear maps for titanium nitride coatings deposited on copper and brass with electroless nickel interlayers, *Wear*, 2000, vol. 241, no. 2, pp. 228–233.
4. Wu, Y., Liu, H., Shen, B., Liu, L., and Hu, W., The friction and wear of electroless Ni–P matrix with PTFE and/or SiC particles composite, *Tribol. Int.,* 2006, vol. 39, no. 6, pp. 553–559.
5. Yan, M., Ying, H.G., and Ma, T.Y., Improved microhardness and wear resistance of the as-deposited electroless Ni–P coating, *Surf. Coat. Tech.*, 2008, vol. 202, no. 24, pp. 5909–5913.
6. Bani-Hani, M., Abd-Allah, R., and El-Khouri, L., Archeaometallurgical finds from Barsinia, Northern Jordan: Microstructural characterization and conservation treatment, *J. Cultur. Heritage*, 2012, vol. 13, no. 3, pp. 314–325.
7. Chen, C.-W., Numerical analysis for the multi-phase flow of pulverized coal injection inside blast furnace tuyere, *Appl. Math. Model.*, 2005, vol. 29, no. 9, pp. 871–884.
8. Malfliet, A., Lotfian, S., Scheunis, L., Petkov, V., Pandelaers, L., Jones, P.T., and Blanpain, B., Degradation mechanisms and use of refractory linings in copper production processes: A critical review, *J. Eur. Ceram. Soc.*, 2014, vol. 34, no. 3, pp. 849–876.
9. Xiong Wei, JIA Juan, Chen Jia-chao, and Shang He-ming, Failure mechanism and material requirements for coal lance in blast furnace, *J. Iron. Steel Res. Int.*, 2012, vol. 19, no. 4, pp. 11–16.
10. Yang Da-zheng, Guan Yong, Zhang Yue, Li Jing, Hu Jun-ge, and Li Wen-zhu, Application of ceramic coat synthesized by in-situ combustion synthesis to BF Tuyere, *J. Iron. Steel Res. Int.*, 2007, vol. 14, no. 2, pp. 70–72.
11. Zhang, F.-m., Design and operation control for long campaign life of blast furnaces, *J. Iron. Steel Res. Int.*, 2013, vol. 20, no. 9, pp. 53–60.
12. Tsaur Charng-Cheng, Rock James, C., Wang Chaur-Jeng, Su Yung-Hua, Tsaur, C.-C., et al., The hot corrosion of 310 stainless steel with pre-coated $NaCl/Na_2SO_4$ mixtures at 750°C, *Mater. Chem. Phys.,* 2005, vol. 89, nos. 2–3, pp. 445–453.
13. Dennis, J.K. and Such, T.E., *Autocatalytic Deposition of Nickel, in Nickel and Chromium Plating*, 2nd Ed., Dennis, J.K. and Such, T.E., Eds., Butterworth-Heinemann, 1986, Ch. 11, pp. 269–285.
14. Mai, Q.X., Daniels, R.D., and Harpalani, H.B., Structural changes induced by heating in electroless nickel phosphorous alloys, in *Metallurgical Coatings*, R.C. Krutenat, Ed., Elsevier, 1988, pp. 235–247.
15. Novak, M., Vojtech, D., Novak, P., and Vitu, T., Tribological properties of heat-treated electroless Ni–P, coatings on AZ91 alloy, *Appl. Surf. Sci.*, 2011, vol. 257, no. 23, pp. 9982–9985.
16. Huang Li-Mei, Luo Lai-Ma, Ding Xiao-Yu, Luo Guang-Nan, Zan Xiang, Cheng Ji-Gui, and Wu Yu-Cheng, Effects of simplified pretreatment process on the morphology of W–Cu composite powder prepared by electroless plating and its sintering characterization, *Powder Technol.,* 2014, vol. 258, no. 0, pp. 216–221.
17. Li, M. and Zinkle, S.J., 4.20—Physical and mechanical properties of copper and copper alloys, in *Comprehensive Nuclear Materials*, Konings, R.J.M., Ed., Oxford: Elsevier, 2012, pp. 667–690.
18. Gu, L., Chen, X., Fan, X., Liu, Y., Zou, B., Wang, Y., and Cao, X., Improvement of thermal shock resistance for thermal barrier coating on aluminum alloy with various electroless interlayers, *Surf. Coat. Tech.*, 2011, vol. 206,no. 1, pp. 29–36.
19. Cui, G., Li, N., Li, D., Zheng, J., and Wu, Q., The physical and electrochemical properties of electroless deposited nickel-phosphorous black coatings, *Surf. Coat. Tech.*, 2006, vol. 200, no. 24, pp. 6808–6814.
20. Elansezhian, R., Ramamoorthy, B., and Kesavan Nair, P., Effect of surfactants on the mechanical properties of electroless (Ni–P) coating, *Surf. Coat. Tech.*, 2008, vol. 203, nos. 5–7, pp. 709–712.
21. Rabizadeh, T., Allahkaram, S.R., and Zarebidaki, A., An investigation on effects of heat treatment on corrosion properties of Ni–P electroless nano-coatings, *Mater. Design.,* 2010, vol. 31, no. 7, pp. 3174–3179.
22. Sahoo, P. and Das, S.K., Tribology of electroless nickel coatings—a review, *Mater. Design.*, 2011, vol. 32, no. 4, pp. 1760–1775.
23. Yang Li-Kun, Jiang Yi-Feng, Yang Fang-Zu, Wu De-Yin, and Tian Zhong-Qun, Phase transformation sequence of mixed-structural electroless Ni–19.7 at % P deposit, *Surf. Coat. Tech.*, 2013, vol. 235, no. 0, pp. 277–282.
24. Mahallawy, N.El., Bakkar, A., Shoeib, M., Palkowski, H., Neubert, V., Mahallawy, N.El., et al., Electroless Ni–P coating of different magnesium alloys, *Surf. Coat. Tech.*, 2008, vol. 202, no. 21, pp. 5151–5157.